Palaeogeography, Palaeoclimatology, Palaeoecology 528 (2019) 232–246

Contents lists available at ScienceDirect

Palaeogeography, Palaeoclimatology, Palaeoecology

journal homepage: www.elsevier.com/locate/palaeo

Paleomagnetism and rock magnetic cyclostratigraphy of the Ediacaran Doushantuo Formation, South China: Constraints on the remagnetization mechanism and the encoding process of Milankovitch cycles

Zheng Gong[a,b,*], Kenneth P. Kodama[b], Yong-Xiang Li[c]

[a] Department of Geology and Geophysics, Yale University, 210 Whitney Avenue, New Haven, CT 06511, USA
[b] Department of Earth and Environmental Sciences, Lehigh University, 1 West Packer Avenue, Bethlehem, PA 18015, USA
[c] State Key Laboratory for Mineral Deposit Research, School of Earth Sciences and Engineering, Nanjing University, 163 Xianlin Avenue, Nanjing 210023, China

ARTICLE INFO

Keywords:
Spectral analysis
Paramagnetic minerals
Chemical remanent magnetization
Chronostratigraphy
Shuram carbon isotope excursion

ABSTRACT

South China provides exceptional and unique sedimentary archives of Earth's fundamental changes in Ediacaran time. However, the lack of robust geochronological constraints renders a poorly-defined chronostratigraphic framework for Ediacaran-aged strata in South China, thus making it difficult to understand Earth's critical changes during this time interval. Magnetostratigraphy and rock magnetic cyclostratigraphy turn out to be a few reliable methods in chronostratigraphic studies, especially in the Precambrian. Here, we present a detailed paleomagnetic and rock magnetic study of the Ediacaran Doushantuo Formation in the Huanglianba section, Guizhou Province, South China. The section consists of ~75 m thick carbonate succession and has a record of one of the largest carbon isotope excursions in the Earth history, known as the Shuram excursion. Stepwise thermal demagnetization of Doushantuo carbonates reveals single-component magnetizations that yield a paleomagnetic pole consistent with the Late Triassic segment of the apparent polar wander path of South China. The secondary origin of Doushantuo carbonates' magnetization is supported by their magnetic mineralogy based on various rock magnetic experiments and scanning electron microscopic analyses. We interpret that the secondary magnetization resides mainly in authigenic pyrrhotite that likely precipitated from the reducing fluids during the late stage of Indosinian orogeny in the Triassic. Interestingly, the companion high-resolution cyclostratigraphic study of a 4-m thick succession at the upper layers of the Doushantuo Formation in the Huanglianba section indicates that the Milankovitch cycles were encoded in the variation of magnetic susceptibility, immune from the influence of remagnetization. Variation of magnetic susceptibility is attributed to changes in the abundance of paramagnetic minerals which, by implication, means that the amount of terrestrial materials transported from the continent was regulated by Milankovitch cycles during the deposition of Doushantuo carbonates. Therefore, our results suggest that even though carbonates are prone to remagnetization, astronomical modulation of deposition could be encoded in rock magnetics of the remagnetized carbonates. As a result, rock magnetic cyclostratigraphy has potential in remagnetized carbonates for providing a floating astronomical timescale that can be applied to constrain sediment accumulation rates, estimate the duration of geological events, and construct high-resolution chronostratigraphies.

1. Introduction

The Ediacaran Period (~635–541 Ma; Knoll et al., 2006) marks Earth's fundamental geological and biological evolutions between the Marinoan glaciation and the Cambrian diversification of multicellular animals. Among other paleocontinents, South China plays an important role in documenting Earth's critical changes in Ediacaran time. The Ediacaran strata in South China have exceptional preservation of metazoan embryos, acanthomorphic acritarchs and multicellular algae (Xiao and Laflamme, 2009), as well as large variations in seawater chemistry which indicate significant transitions in oceanic and atmospheric redox conditions (e.g., McFadden et al., 2008; Li et al., 2010; Xiao et al., 2012; Kendall et al., 2015; Shi et al., 2018). Additionally, high-precision U–Pb geochronology from the volcanic ash layers in South China (e.g., Condon et al., 2005; Zhang et al., 2005) provides key age constraints for worldwide stratigraphic comparisons and

* Corresponding author at: Department of Geology and Geophysics, Yale University, 210 Whitney Avenue, New Haven, CT 06511, USA.
E-mail address: z.gong@yale.edu (Z. Gong).

https://doi.org/10.1016/j.palaeo.2019.05.002
Received 23 November 2018; Received in revised form 14 March 2019; Accepted 1 May 2019
Available online 11 May 2019
0031-0182/

correlations.

Because it is difficult to apply biostratigraphy to correlate sedimentary sequences globally prior to the widespread appearance of cosmopolitan fossils, magnetostratigraphy serves as one of a few reliable methods that can provide a chronostratigraphic framework for the Ediacaran strata. However, paleomagnetic studies in South China face three major challenges. First, the Ediacaran strata in South China are dominated by carbonates (Zhu et al., 2007), which are susceptible to both thermal and chemical alterations. Hence, the magnetization preserved in carbonates often have a complicated origin and the primary signal usually suffers from post-depositional overprints to various degrees (e.g., McCabe and Elmore, 1989). Second, South China has experienced multiple episodes of Phanerozoic tectonic activities, therefore some pre-Mesozoic structures could have been partially or completely overprinted (e.g., Wang et al., 2013). Third, it has been suggested that the geomagnetic field in Ediacaran time was not stable and had transient non-geocentric-axial-dipole (GAD) behaviors intermittently (Abrajevitch and Van der Voo, 2010), increasing the difficulty of a straightforward interpretation and application of paleomagnetic data, especially without reliable age constraints. As a result of these challenges, reliable paleomagnetic data from the Ediacaran strata in South China are scarce, pointing to the necessity for more work.

In addition to magnetostratigraphy, the newly developed rock magnetic cyclostratigraphy is shown to be a promising technique to assign a high-resolution (~ tens of thousands of years) chronostratigraphy to sedimentary sequences (Kodama and Hinnov, 2014), and has been successfully applied to various geological settings from the recent back to Mesoproterozoic time (e.g., Kodama et al., 2010; Gunderson et al., 2013; Wu et al., 2012; Minguez et al., 2015; Bao et al., 2018; Zhang et al., 2015). Rock magnetic parameters are determined by the variations in the concentration or the type of magnetic minerals in sedimentary rocks. Recently, magnetic susceptibility (MS) is widely used to determine a rock magnetic cyclostratigraphy. MS could be carried by a combination of paramagnetic, diamagnetic and ferromagnetic minerals, and could be immune from the remagnetizing processes that would erase the primary magnetization. Depending on the specific remagnetization mechanism and the encoding process of Milankovitch cycles, rock magnetic cyclostratigraphy can still be useful in remagnetized sedimentary rocks. For example, Gong et al. (2017) show that Milankovitch cycles could be primarily encoded by the variation in MS, even though the rocks carry a thermoviscous remagnetization. Therefore, rock magnetics need to be rigorously studied before the application of rock magnetic cyclostratigraphy, especially when dealing with ancient sedimentary rocks.

Here, we present a detailed study of the Ediacaran Doushantuo Formation in the Huanglianba section, Songtao County, Guizhou Province, South China, combining paleomagnetism, rock magnetism, and scanning electron microscopy (SEM) to evaluate the age and origin of the magnetization. Also, we report a rock magnetic cyclostratigraphy using MS in Doushantuo carbonates. We show that the cycles observed in MS series correspond to astronomically forced climate cycles (Milankovitch cycles) and discuss the encoding processes of climate cycles by rock magnetics. We also discuss the potential of rock magnetic cyclostratigraphy in chronostratigraphic studies in ancient sedimentary rocks.

2. Geological background and sampling

South China was amalgamated by the collision between the Yangtze Block and the Cathaysia Block at ~900 Ma (Fig. 1A; e.g., Li et al., 2007). Following the final breakup of the supercontinent Rodinia and two Cryogenian Snowball Earth events, the Ediacaran strata in South China were deposited on a passive continental margin, mainly consisting of several-hundred-meter thick, interbedded carbonates and siliciclastic rocks on the Yangtze Platform stratigraphically overlying above the Marinoan diamictites (Nantuo Formation). The Ediacaran strata are composed of two units, the lower Doushantuo Formation and the upper Dengying/Liuchapo Formation. The Doushantuo-Dengying/Liuchapo boundary is characterized by the transition from the Doushantuo black shales to the Dengying dolostones and is precisely dated to be 551.1 ± 0.7 Ma by U–Pb geochronology of zircons in an ash layer in the Three Gorges area (Condon et al., 2005). Detailed sequence stratigraphy work further divides the fossiliferous Doushantuo Formation into four members (Jiang et al., 2011), with the distinctive cap carbonate layer (Member I) at the bottom of the formation, the interbedded shale and carbonate layers (Member II), the carbonate dominated layers (Member III), and the black shale layer at the top (Member IV). The Huanglianba section is located in Songtao County in Guizhou Province (28°11′28.5″N, 109°15′58.5″E), which was deposited in a slope environment of the Yangtze Platform (Fig. 1B; Jiang et al., 2011). The lithology of the Huanglianba section has been carefully characterized by Lu et al. (2013). Based on their description and our field observation, the Doushantuo Formation here is ~75 m thick and outcrops between the Nantuo diamictites and the Liuchapo thinly-bedded chert layers (Fig. 1C). The Doushantuo Formation consists of 6-m thick cap carbonates, 4-m of mixed dolostones and black shales, 40-m of thinly-bedded banded limestones, and a 25-m mixture of shales and thinly-bedded cherts and dolostones (Fig. 1C). Soft-sediment deformation (e.g., slump folds) has been observed in the field and also noted in Lu et al. (2013) in the Huanglianba section (Fig. 1F), which is a common feature for the slope environment in the Yangtze Platform. Carbon isotopic study has also been reported in Lu et al. (2013). The $\delta^{13}C_{VPDB}$ values of the cap carbonates are ~−3 ‰, which are typical for such a lithology and comparable to time-equivalent cap carbonates globally (Halverson et al., 2005). Upsection, the $\delta^{13}C_{VPDB}$ values decrease sharply to ~−9‰, and persist at such depleted values for about 50 m before returning to ~−2‰ (Fig. 1D). The remarkably depleted $\delta^{13}C_{VPDB}$ signatures are comparable to the well-known Shuram carbon isotope excursion (CIE; Grotzinger et al., 2011), and this section has been correlated to other time-equivalent sections based on lithology and carbon isotopic stratigraphy across the Yangtze Platform and globally (Lu et al., 2013). Structurally, the Doushantuo Formation in the Huanglianba section is gently tilted easterly at about 20°, and according to geological investigations of this region, the tilting is Late Mesozoic in age and related to the Yanshanian orogeny in South China (BGMRGP, 1987).

Paleomagnetic sampling was conducted using a gasoline-powered portable drill to collect oriented cores, starting at the boundary between the Nantuo diamictites and the Doushantuo cap carbonates (Fig. 1C). Slump folds were avoided because they indicate disturbance of the sedimentation before lithification. A total of 12 sites were collected with an average sampling interval of ~3–4 m (Fig. 1C). Oriented cores were trimmed by an ASC diamond, dual-bladed saw to obtain standard-size paleomagnetic specimens (2.2 cm in length and 2.5 cm in diameter). In the upper section of the thinly-bedded banded limestone layer where the Shuram CIE is located, we observed cyclic color variation of the carbonates (Fig. 1E), which were also noted in the report of a local geological survey (J. Zhang, pers. comm.). Based on similar work from North America, South Australia and South China (Minguez et al., 2015; Minguez and Kodama, 2017; Gong et al., 2017), we collected a total of 200 unoriented samples (about 3–8 cm^3 in size) for a study of rock magnetic cyclostratigraphy. Samples cover a stratigraphic thickness of 4 m with a sampling interval of 0.02 m. The purposes of rock magnetic cyclostratigraphic are to try to understand if the cyclic color variation of carbonates is related to astronomically forced climate cycles, and if rock magnetic cyclostratigraphy could be able to provide an estimate of the sediment accumulation rate (SAR) of Doushantuo carbonates, and further to provide constraints on the duration of the Shuram CIE. A total of 20 samples were selected from the 200 unoriented cyclostratigraphic samples for carbon isotopic measurements.

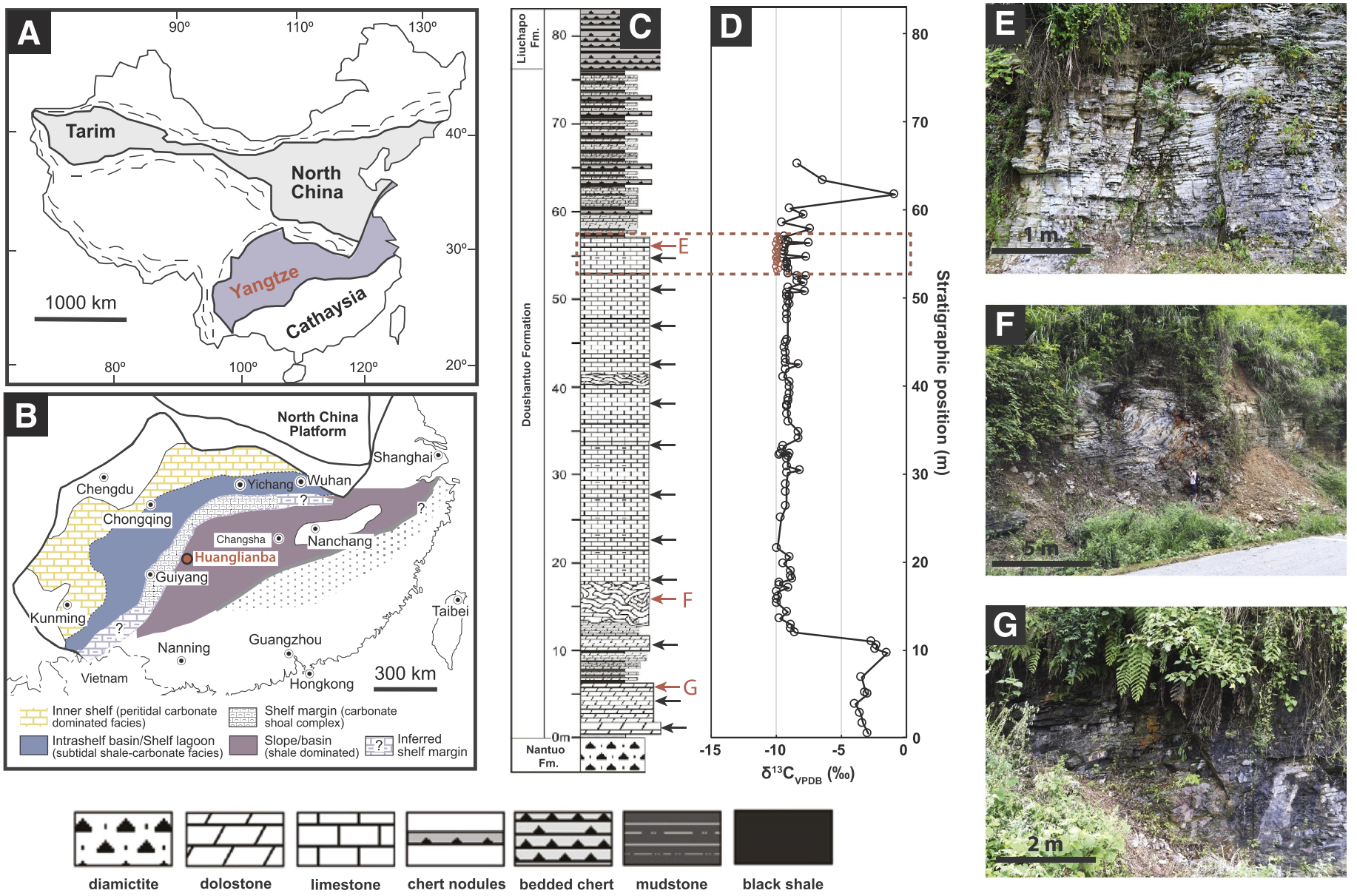

Fig. 1. (A) Geologic map of China, showing the position of the Yangtze Block with respect to other major tectonic blocks of China (Jiang et al., 2011). (B) Depositional environment reconstruction of the Yangtze carbonate platform in Ediacaran time, with the location of the Huanglianba section indicated by a red circle (modified from Jiang et al., 2011). (C) Stratigraphic column of the Ediacaran strata of the Huanglianba section (Lu et al., 2013). Lithologic legends are shown below. Black arrows point to the stratigraphic positions of paleomagnetic sampling sites. Red arrows show the stratigraphic positions of field photographs. (D) Carbon isotope profile. Black open circles are $\delta^{13}C_{VPDB}$ data from Lu et al. (2013). Red open circles are data of this study. Red dashed box marks the stratigraphic positions of cyclostratigraphic samples. (E) Cyclic color variation of carbonate rocks at the top of the Shuram CIE. (F) A slump fold at the base of the Shuram CIE. (G) Basal part of the Doushantuo Formation. (For interpretation of the references to color in this figure legend, the reader is referred to the web version of this article.)

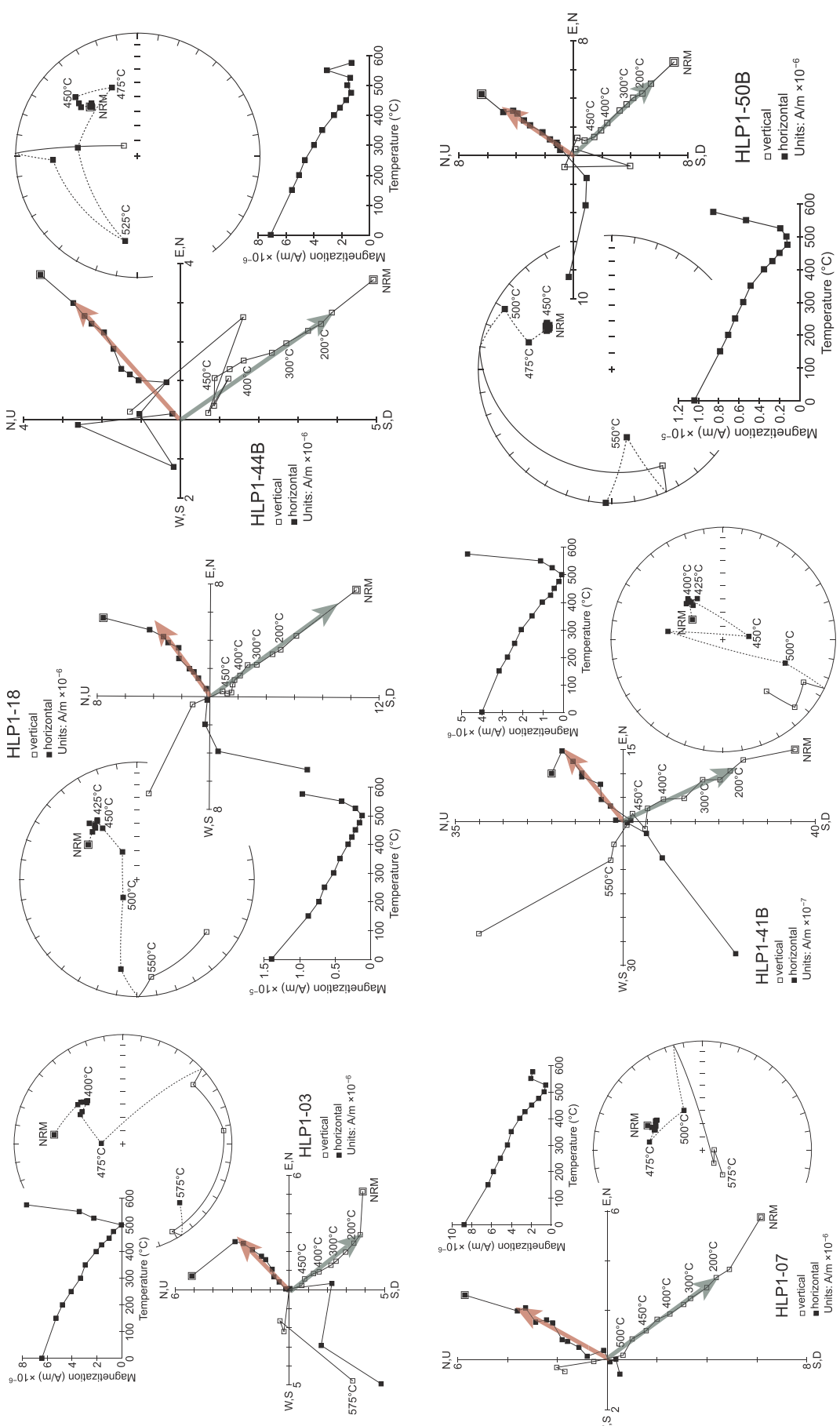

Fig. 2. Representative thermal demagnetization data. Data are in stratigraphic coordinates and are plotted in vector-endpoint diagrams (Zijderveld, 1967), equal-area stereographic projection and magnetization intensity versus temperature curves. The characteristic remanent magnetizations were determined by principal component analysis (Kirschvink, 1980), with red and green arrows showing horizontal and vertical components, respectively. (For interpretation of the references to color in this figure legend, the reader is referred to the web version of this article.)

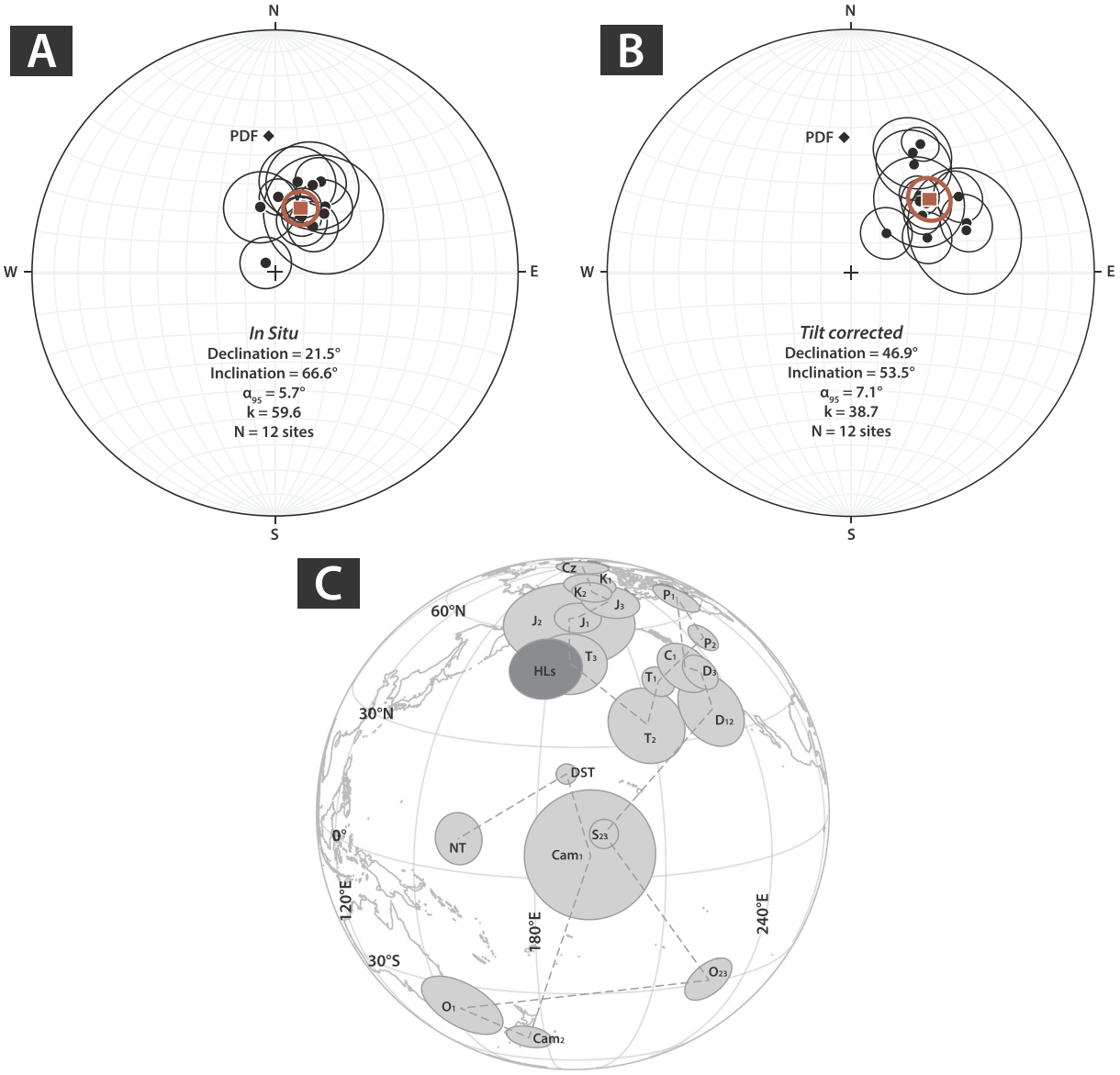

Fig. 3. (A) Equal-area stereographic projection of in-situ paleomagnetic results. (B) Equal-area stereographic projection of tilt-corrected paleomagnetic results. Black circles are mean directions of 12 sites, with the corresponding 95% confidence cones. Red square is the mean of the 12 site means. Paleomagnetic statistics are listed below. PDF is the present-day field direction (black diamond) of the Huanglianba section. (C) APW path of South China, selective paleomagnetic poles are listed in Zhang et al. (2015) and references therein. Paleomagnetic pole obtained from the Huanglianba section is shown using a dark grey oval. HLs = tilt-corrected Huanglianba pole, NT = Nantuo Formation, DST = Doushantuo Formation, Cam = Cambrian, O = Ordovician, S = Silurian, D = Devonian, C = Carboniferous, P = Permian, T = Triassic, J = Jurassic, K = Cretaceous, Cz = Cenozoic. Subscripts 1, 2, 3 mean early, middle and late Epochs, respectively. (For interpretation of the references to color in this figure legend, the reader is referred to the web version of this article.)

3. Methods

The measurement of remanent magnetization was performed with a 2G Enterprises 755 superconducting rock magnetometer stationed in the magnetostatically-shielded (residual field < 350 nT) Paleomagnetism Laboratory at Lehigh University. After the natural remanent magnetization (NRM) of each specimen was measured, stepwise thermal demagnetization was applied, typically at 150 °C, 200 °C, 250 °C, 300 °C, 350 °C, 400 °C, 425 °C, 450 °C, 475 °C, 500 °C, 525 °C, 550 °C, 575 °C in 13 steps using an ASC Model TD-48SC thermal demagnetizer. The characteristic remanent magnetization (ChRM) of each specimen was isolated by principal component analysis (Kirschvink, 1980) on vector-endpoint diagrams (Zijderveld, 1967) in PuffinPlot software (Lurcock and Wilson, 2012). Paleomagnetic mean directions were calculated using Fisher statistics (Fisher, 1953). Representative samples were further subjected to a series of rock magnetic experiments for magnetic mineralogy identification. Isothermal remanent magnetization (IRM) was applied sequentially from 4 mT up to 1.2 T in 26 steps by an ASC impulse magnetometer. IRM acquisition curves were then modeled by several coercivity components following Kruiver et al. (2001). IRM was also applied in three orthogonal axes of representative samples in three different field ranges, specifically 0–0.1 T along the X axis, 0.1–0.6 T along the Y axis and 0.6–1.2 T along the Z axis. Then thermal demagnetization of three orthogonal IRMs was carried out (Lowrie test; Lowrie, 1990). Low-temperature MS was measured on representative powdered samples, which were cooled to liquid nitrogen temperature (~77 K) and slowly warmed to room temperature (~300 K) using an AGICO Kappabridge KLY-3S susceptibility meter. To investigate the mineralogy and morphology of magnetic grains, we performed SEM studies on the powdered samples using a Thermo

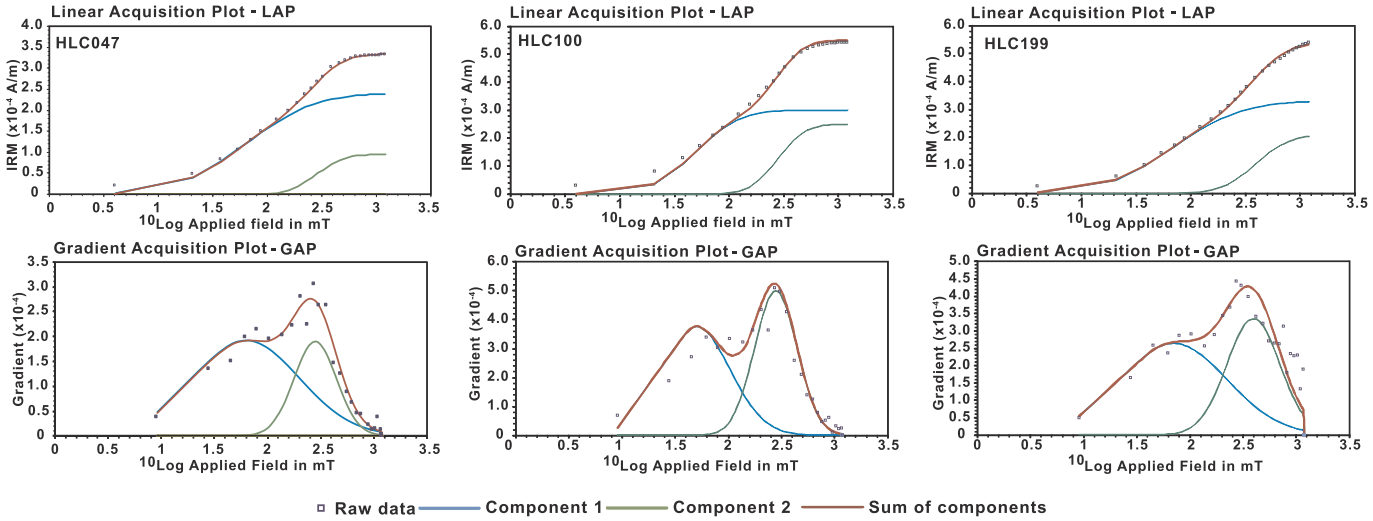

Fig. 4. Modeling results of representative curves of IRM acquisition experiments show two magnetic coercivity components (Kruiver et al., 2001). Modeling data are listed in Table 1.

Table 1
Modeling results of the acquisition curve of IRM and deduced magnetic mineralogy.

	Component	Contribution (%)	SIRM (A/m)	log $B_{1/2}$ (mT)	$B_{1/2}$ (mT)	DP (mT)	Mineralogy
HLC047	1	71.6	2.4×10^{-4}	1.80	63.1	0.50	Magnetite
	2	28.4	9.5×10^{-5}	2.45	281.8	0.20	Pyrrhotite
HLC100	1	54.5	3.0×10^{-4}	1.70	50.1	0.32	Magnetite
	2	45.5	2.5×10^{-4}	2.45	281.8	0.20	Pyrrhotite
HLC199	1	61.1	3.3×10^{-4}	1.85	70.8	0.50	Magnetite
	2	38.9	2.1×10^{-4}	2.60	398.1	0.25	Pyrrhotite

Note: $B_{1/2}$ = mean coercivity, DP = half-width of the distribution.

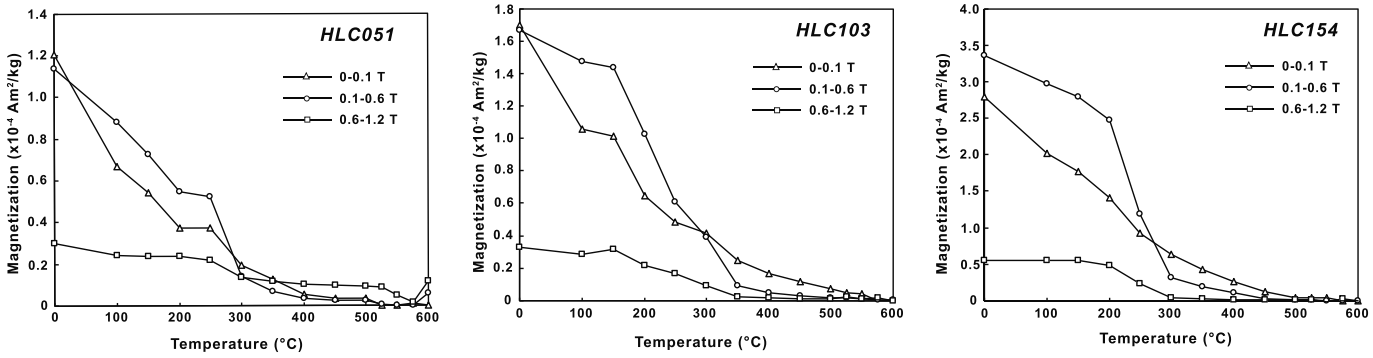

Fig. 5. Representative results of thermal demagnetization of three orthogonal IRMs (Lowrie, 1990). Magnetic coercivity ranges are 0–0.1 T (triangles), 0.1–0.6 T (open circles) and 0.6–1.2 T (squares) in three orthogonal axes, respectively.

Scientific Phenom XL Desktop SEM operating at 15 keV, and used an energy dispersive spectrometer (EDS) for stoichiometric analysis.

We measured the MS at room temperature of a total of 200 cyclostratigraphic samples. MS values are the averages of three repeated measurements and then mass-normalized before spectral analysis. To study the frequencies of cyclic patterns in MS series, we removed the linear trend of the dataset, and performed the 3π multi-taper method (MTM) spectral analysis of MS series (Thomson, 1982) using Astrochron R package (Meyers, 2014). Robust red noise, along with the associated 90%, 95% and 99% confidence levels was calculated following Mann and Lees (1996) to determine statistically significant spectral peaks. Average spectral misfit (ASM) analysis was also conducted to obtain the optimal SAR (Meyers and Sageman, 2007) of the stratigraphic interval that we sampled for rock magnetic cyclostratigraphy. Target astronomical frequencies (2 short eccentricities, 1 obliquity and 4 precessions) for ASM analysis were used based on the calculations of Laskar et al. (2004) and Waltham (2015) for the Ediacaran time.

Carbon isotope values were measured and compared with a previous study (Lu et al., 2013), which will help precisely locate the stratigraphic position of the cyclostratigraphic samples in addition to the section measurement in the field. A total of 20 whole-rock powdered samples were prepared using fresh rock chips of the cyclostratigraphic samples with an agate mortar and pestle. Powders were acidified with 100% H_3PO_4 at 70 °C on a Gas Bench II for 2 h, and a Finnigan MAT252 mass spectrometer was used for carbon isotopic measurements in the Stable Isotope Laboratory at Lehigh University. International standard NBS19 and a house standard were used for calibration. All carbon isotopic values are reported compared to the Vienna Pee Dee Belemnite (VPDB).

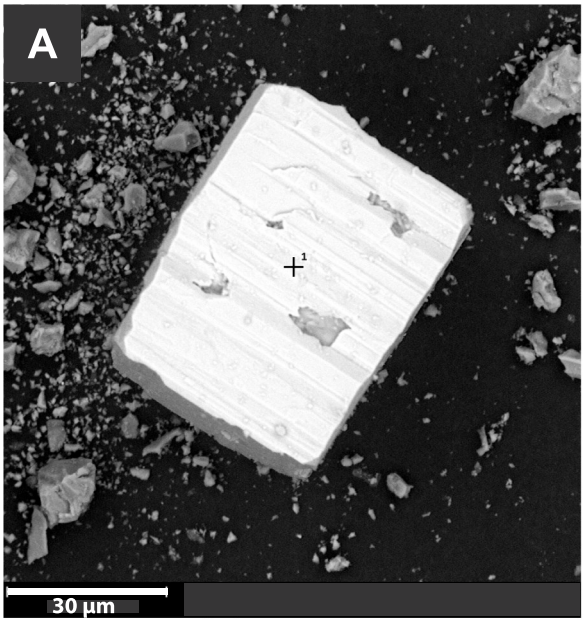

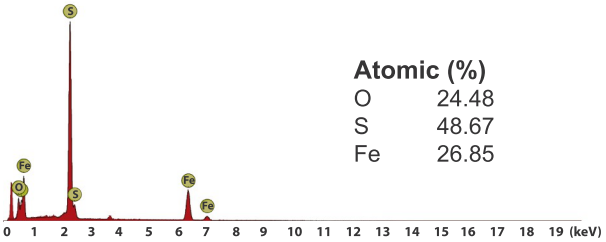

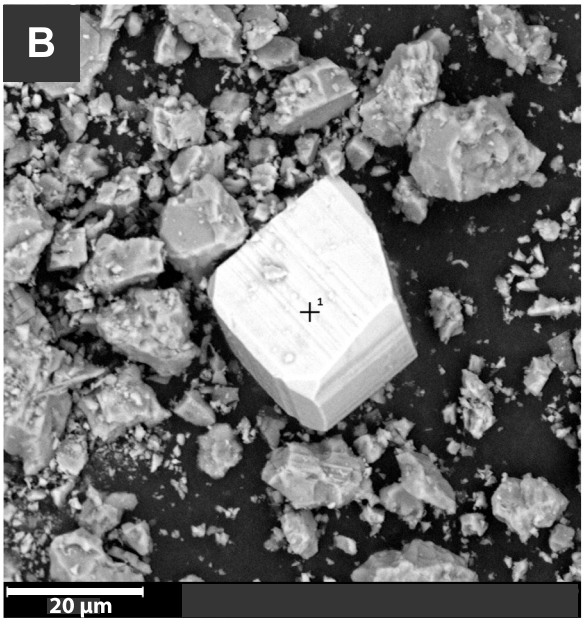

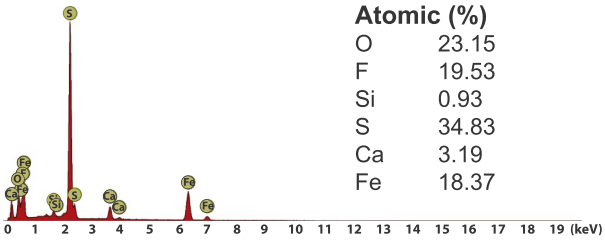

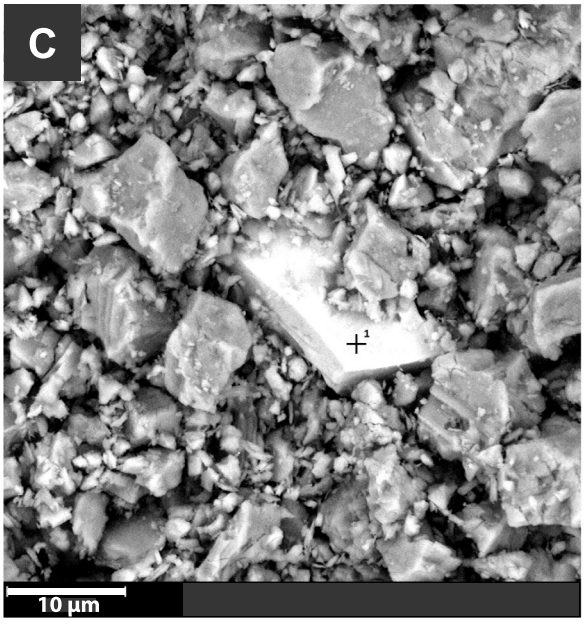

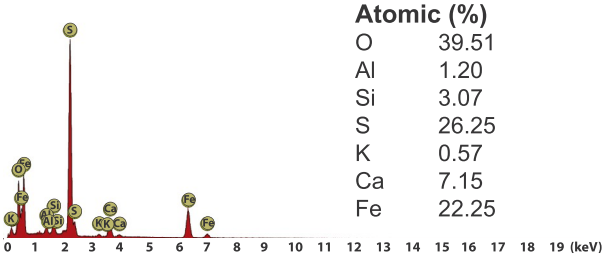

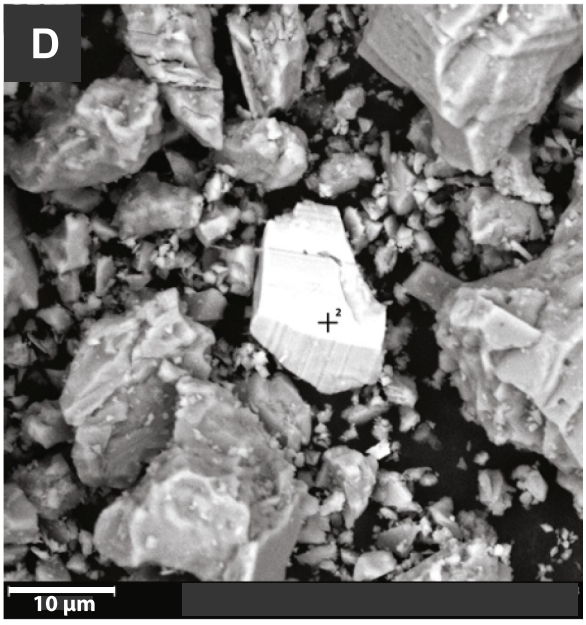

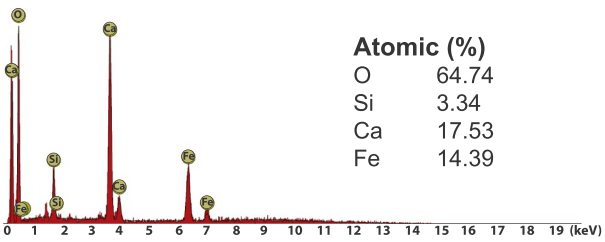

(caption on next page)

Fig. 6. SEM images and EDS spectra of iron-bearing minerals. (A) and (B) show pyrite (FeS_2), (C) shows pyrrhotite (Fe_7S_8), and (D) shows magnetite (Fe_3O_4). Chemical formula of magnetic sulfides is based on the morphology and the semi-quantitative ratio of Fe and S.

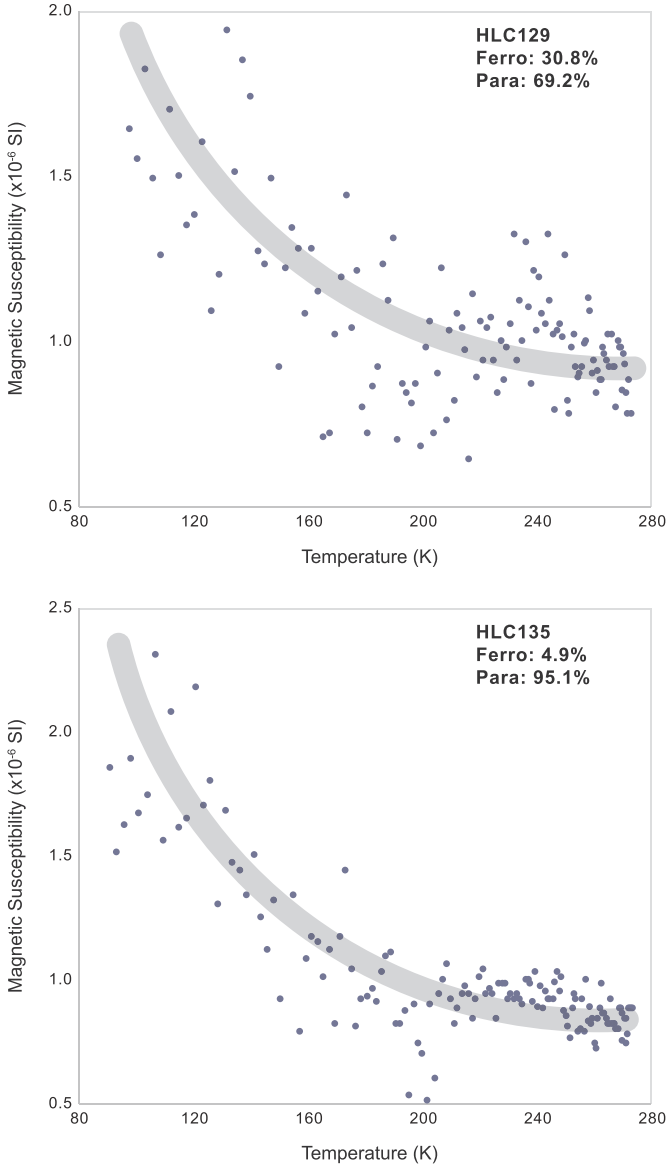

Fig. 7. MS versus temperature curves. The hyperbolic fit following Hrouda et al. (1997) was calculated to resolve the ferromagnetic and paramagnetic contributions to susceptibility.

4. Results

NRM values of the Huanglianba samples range from 1.0×10^{-6} A/m to 3.4×10^{-5} A/m, with a mean value of 7.4×10^{-6} A/m. Results of thermal demagnetization show that the remanent magnetization of Huanglianba samples gradually decreases as temperature increases, then reaches the minimum at ~500 °C, and starts to increase sharply up to 575 °C (Fig. 2), This phenomenon indicates the chemical alteration of magnetic minerals during heating. Pyrrhotite breaks down to magnetite at ~500 °C (Dunlop and Özdemir, 2001), which could be the cause for the increase of remanent magnetization above 500 °C. It is noticed that remanent magnetization also becomes unstable at temperatures higher than 450 °C (Fig. 2). Using principal component analysis, we obtained the ChRM of each specimen, typically between 150 °C and 450 °C. All 12 sites give similar site-mean directions, and the mean direction of all site means for the Huanglianba section is Dec. = 21.5°, Inc. = 66.6°, α_{95} = 5.7°, k = 59.6 in geographic coordinates (Fig. 3A). After tilt correction, the mean direction becomes Dec. = 46.9°, Inc. = 53.5°, α_{95} = 7.1°, k = 38.7 (Fig. 3B), which gives a corresponding paleomagnetic pole at Plat. = 49.8°N, Plon. = 178.8°E, A_{95} = 8.3° (Fig. 3C).

IRM acquisition curves show that most samples reach saturation of remanent magnetization at 0.6 T, with only a few samples not fully saturated at 1.2 T (Fig. 4). IRM acquisition curves can be modeled by a combination of two magnetic components, a soft component with an average coercivity of ~60 mT and a hard component with an average coercivity of 300 mT (Fig. 4; Table 1). The coercivities of these two components correspond to the typical values for magnetite and pyrrhotite (Peters and Dekkers, 2003). Lowrie tests show that the remanent magnetization of the intermediate coercivity component (0.1–0.6 T) drops significantly between 250 °C and 350 °C, while the remanent magnetization of the soft coercivity component (0–0.1 T) gradually decreases (Fig. 5). The remanent magnetization of the hard coercivity component (0.6–1.2 T) also shows a minor but noticeable loss around 300 °C (Fig. 5). The temperature range of 250–350 °C is similar to the unblocking temperature of pyrrhotite (Dekkers, 1989). Magnetic sulfides have been observed under the SEM (Fig. 6). Based on the semi-quantitative stoichiometric analysis by EDS, these sulfides are pyrite (FeS_2) and pyrrhotite (Fe_7S_8). Pyrite crystals are cubic in structure with a mean diameter of ~20–30 μm (Fig. 6A and B). There are also sparse mm-sized pyrite crystals which can be recognized by the naked eye in block samples. Pyrrhotite crystals are ~10 μm in size, pseudohexagonal and platy in shape (Fig. 6C), and are likely authigenic since surface weathering could readily cause oxidation of the pyrrhotite. We also observed magnetite (Fe_3O_4) grains (Fig. 6D), which are ~10 μm in size and are characterized as multidomain (MD) grains.

Low-temperature MS measurements indicate that susceptibility decreases with temperature increasing from 80 K to 280 K (Fig. 7), following the relationship between susceptibility and temperature for the Curie law of paramagnetic susceptibility (Butler, 1992):

$$\chi = \frac{J}{H} = \frac{NM^2}{3kT} \quad (1)$$

where J is the induced magnetization, H is the applied field, N is the total number of atomic moments, M is the aligning energy of a magnetic moment, k is the Boltzmann's constant, and T is temperature in Kelvin. Using the hyperbolic fit following Hrouda et al. (1997), we separated ferromagnetic and paramagnetic contributions to MS. Results show that paramagnetic minerals dominate the magnetic phases in Huanglianba samples, with varying contributions of ~70–95% (Fig. 7).

Carbon isotopic values of the cyclostratigraphic samples are between −10‰ and −9‰, in a good agreement with the previous study (Fig. 1D; Lu et al., 2013). Cyclostratigraphic sampling interval is 0.02 m, which yields a Nyquist frequency of 25 m^{-1} and a Rayleigh frequency of 0.25 m^{-1}, and allows a wide-range detection of signals. MTM spectral analysis of MS series reveals a number of peaks that are above the 90% confidence level (Fig. 8B). The frequencies of these six statistically significant peaks are specifically at 1.28 m^{-1}, 3.30 m^{-1}, 5.53 m^{-1}, 7.12 m^{-1}, 19.03 m^{-1} and 20.03 m^{-1} (Fig. 8B; Table 2). In order to determine if these peaks are related to astronomically forced climate cycles, we performed ASM analysis (Fig. 9; Meyers and Sageman, 2007), assigning the spectral peak with the frequency of 1.28 m^{-1} to short eccentricities (123.9 kyr and 94.9 kyr), the spectral peak with the frequency of 3.30 m^{-1} to obliquity (31,8 kyr), and the spectral peaks with the frequencies of 5.53 m^{-1} and 7.12 m^{-1} to precessions (20.2 kyr, 19.2 kyr, 16.8 kyr and 16.6 kyr), respectively. The periodicities of target astronomical cycles are estimated by Laskar et al. (2004) for short eccentricities, and by Waltham (2015) for obliquity

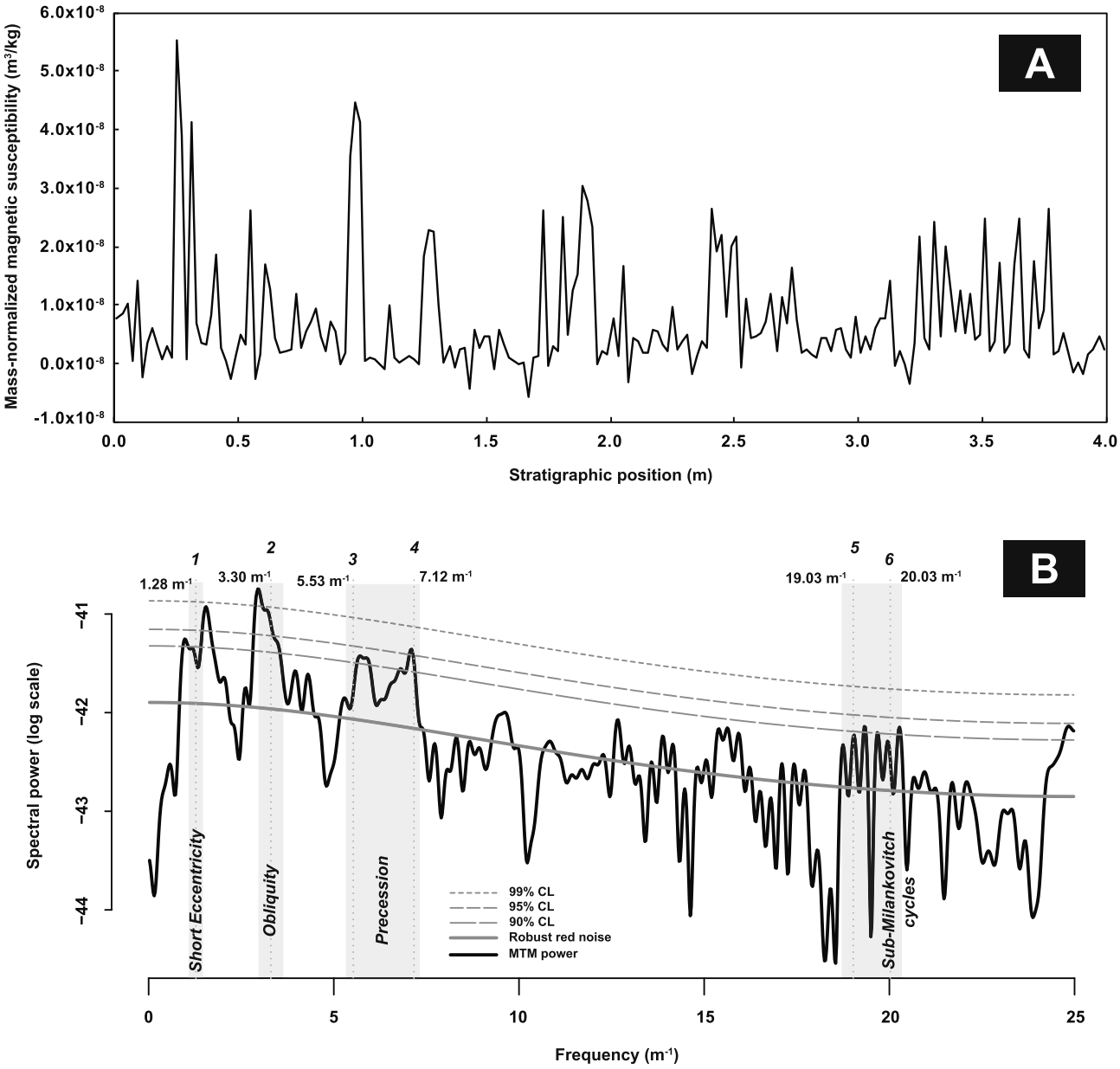

Fig. 8. (A) 4-m raw mass-normalized MS series, with a sampling interval of 0.02 m. (B) 3π MTM power spectrum with significant harmonic lines using "mtmML96" function with robust red noise (Mann and Lees, 1996) in Astrochron R package (Meyers, 2014). The significant peaks are numbered with their frequencies shown. CL = confidence level. (For interpretation of the references to color in this figure legend, the reader is referred to the web version of this article.)

Table 2
Results of the MTM spectral analysis.

Milankovitch cycles		Short eccentricity	Obliquity	Precession		Sub-Milankovitch cycles		Ratio
Theoretical astronomical periodicity (kyr)		94.9[a]	31.8 ± 4.3[b]	20.2 ± 1.7[b]	16.6 ± 1.2[b]	–	–	5.7:1.9:1.2:1
Significant peaks	Frequency (m^{-1})	1.28	3.30	5.53	7.12	19.03	20.03	–
	Wavelength (cm)	78.13	30.30	18.08	14.04	5.25	4.99	5.6:2.2:1.3:1
	Periodicity (kyr)	90.84	35.24	21.03	16.33	6.11	5.81	–
Sediment accumulation rate (cm/kyr)		0.86						

[a] From Laskar et al. (2004).
[b] From Waltham (2015)'s theoretical estimates at 560 Ma.

and precessions at 560 Ma. The minimum misfit is achieved with a SAR of 0.86 cm/kyr, with a low *p*-value of 4×10^{-5}. The p-value is well below the critical significance level (Fig. 9B), so that the null hypothesis which the spectral peaks are not astronomical cycles can be rejected with high confidence.

5. Discussion

5.1. Remagnetization mechanism

One of the main findings of this study is that the Ediacaran

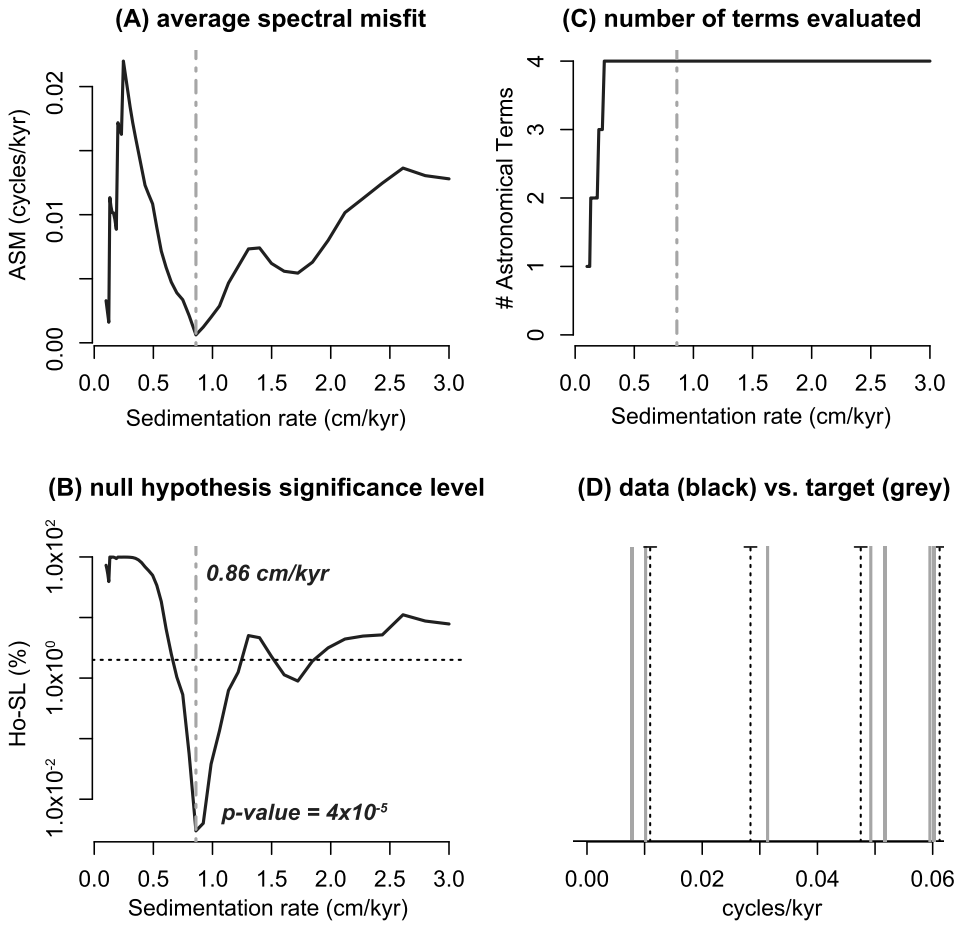

Fig. 9. ASM results using "asm" function in Astrochron R package (Meyers, 2014). Grey vertical dashed lines in (A) and (B) are the absolute minimum misfit sedimentation rates. Black horizontal dotted line is the H_0 "critical significance level" needed to reject the null hypothesis of no astronomical signal. (C) Number of frequencies used to evaluate sedimentation rates between 0.1 cm/kyr and 3.0 cm/kyr. (D) The significant frequencies (dashed lines) compared with the target Milankovitch frequencies (grey lines).

Doushantuo carbonates in the Huanglianba section appear to be completely remagnetized in Late Triassic time. The paleomagnetic pole obtained after tilt-corrected mean paleomagnetic direction is similar to the Late Triassic segment of South China's APW path (Fig. 3C). We argue that the remagnetization could likely be related to the Indosinian orogeny which resulted from the collision between the North China Block and the South China Block from the end-Permian to through the Triassic.

Rock magnetic experiments and SEM analyses provide additional lines of evidence for the Triassic remagnetization, and help explain its mechanism. The ChRMs of Huanglianba samples are isolated at temperatures (150–450 °C) lower than the typical unblocking temperature of Ti-poor, single-domain (SD) magnetite (Fig. 2), which is expected to be between 500 °C and 580 °C (Dunlop and Özdemir, 2001). IRM modeling and the Lowrie test indicate the presence of pyrrhotite (Figs. 4 and 5), which is further confirmed by SEM and EDS analyses (Fig. 6). Hence, pyrrhotite is believed to be the main carrier of the ChRMs. There is also evidence for the existence of magnetite, which is MD in size and is likely detrital based on the morphology (Fig. 6D). Geothermal temperature estimates by source rock maturity characterization show that the lower Cambrian carbonates experienced ~220 °C heating during the Jurassic before exhumation in the sampling area (Han et al., 2013). Hence, the geothermal temperature of the Ediacaran strata should be at least over 220 °C. According to Pullaiah et al. (1975)'s theoretical calculations, SD magnetite could be subject to a thermoviscous remagnetization at 220 °C during a 10 Myr interval of heating that requires thermal demagnetization at 450 °C for 1 h in the laboratory. Therefore, MD magnetite, which is less stable than SD magnetite, could carry the thermoviscous remanent magnetization when the hot reducing fluid was migrating through the strata during the Indosinian orogeny and remagnetizing the carbonates. This explains the consistent ChRM directions between 150 °C and 450 °C, ~100 °C higher than the Curie temperature of pyrrhotite. The primary remanent magnetization is completely obscured by the chemical remagnetization carried by pyrrhotite, with minor contributions of thermoviscous remagnetization carried by MD, detrital magnetite. It is difficult to resolve the primary remanent magnetization because pyrrhotite breaks down to magnetite at ~500 °C (Dunlop and Özdemir, 2001). Pyrite was also observed under SEM, which shows large, cubic and euhedral crystal structures (Fig. 6), indicating an authigenic origin. We argue that during the Indosinian orogeny, pyrite was precipitated from the reducing fluids that were chemically reactive. Pyrrhotite was the intermediate product of the reduction and was magnetized in the ambient field of Late Triassic time. Therefore, the remagnetization is chemical in origin.

Triassic-aged chemical remagnetization has also been observed in Late Cambrian carbonates and Silurian shales in South China (Jiao et al., 2018; Jiao et al., 2019; Zhang et al., 2016). When combining the geography and the age of remagnetization of the studied sections, Jiao et al. (2019) noticed that there is a westward younging of the Triassic remagnetization (Fig. 10A). Specifically, the Late Cambrian carbonates in Zhejiang Province carry an Early-Middle Triassic remagnetization (Jiao et al., 2018). Moving westwards to Hunan Province, the remagnetization of the Late Cambrian carbonates becomes younger, i.e. Middle Triassic based on the position of the paleomagnetic pole on South China's APW path (Fig. 10B; Jiao et al., 2019). Finally, in Sichuan Province, the Silurian shales exhibit a Late Triassic remagnetization (Zhang et al., 2016). Interestingly, all Triassic remagnetizations are suggested to be chemical in origin and related to the migration of the reducing fluids during the Indosinian orogeny. Considering that the Indosinian orogeny is characterized by the westward suturing between the North China Block and the South China Block (Zhao and Coe, 1987), Jiao et al. (2019) proposed that the orogenic fluids were migrating from

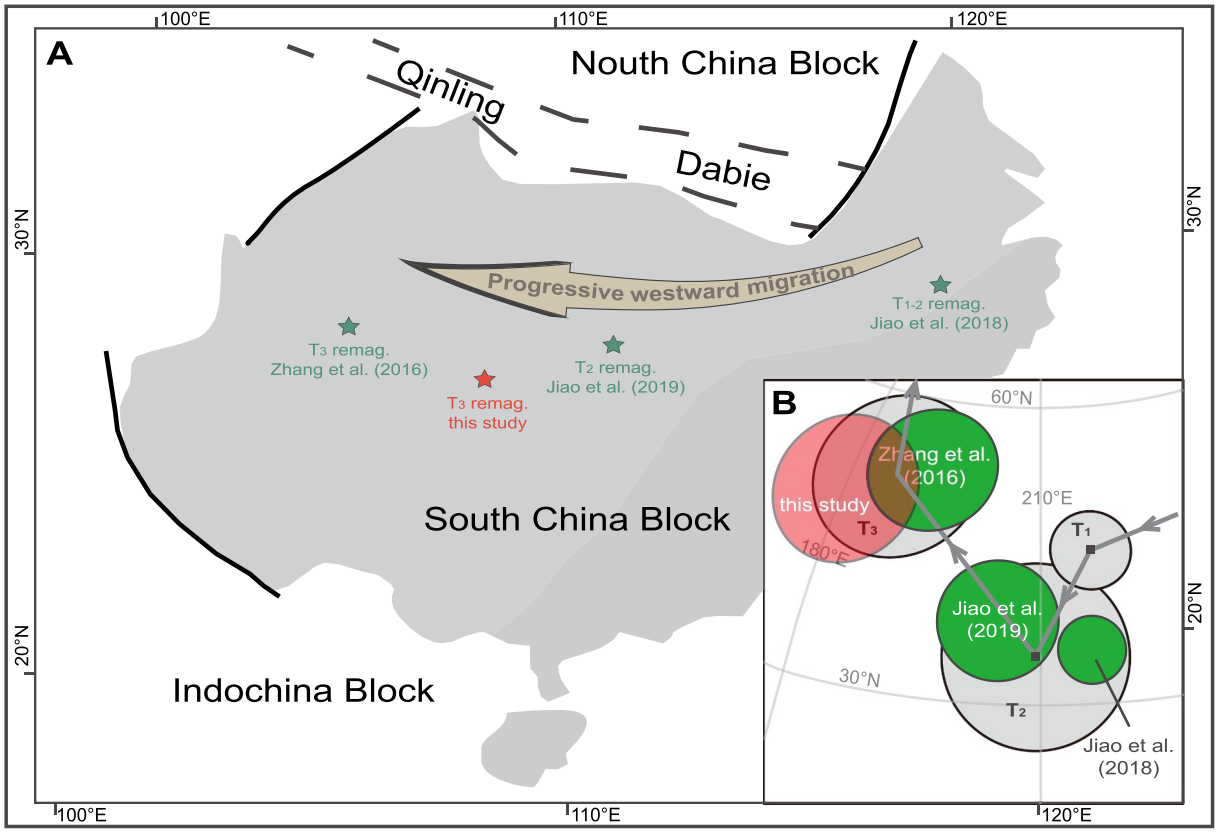

Fig. 10. (A) Schematic South China map showing the westward younging of Triassic-aged chemical remagnetization in four sections. T = Triassic, Subscripts 1, 2, 3 mean early, middle and late Epochs, respectively. (B) Corresponding paleomagnetic poles with respect to the APW path of South China. Modified from Jiao et al. (2019).

the east to the west, which resulted in the westward younging of Triassic remagnetization of Late Cambrian and Silurian strata in South China. If the model of Jiao et al. (2019) is correct, samples from the Huanglianba section, which is located geographically between the Hunan and Sichuan Provinces (Fig. 10), are expected to carry a Late Triassic remagnetization. The Late Triassic remagnetization recognized by our paleomagnetic study agrees well with Jiao et al. (2019)'s model, indicating that the reducing fluids associated with the Triassic Indosinian orogeny might pervasively affect large volume of Neoproterozoic-Paleozoic strata across the entire South China Block.

Most paleomagnetic data from the Doushantuo Formation in South China, unfortunately, reveal remagnetizations of various ages and via different mechanisms (Gong et al., 2017; Jing et al., 2018). Besides Triassic remagnetization, other most commonly observed remagnetizations of Doushantuo carbonates are of Silurian or Late Mesozoic in age, or the combination of these two. But there seems to have no systematic geographic or tectonic controls regarding the age or the mechanism of the remagnetizations, which could probably be due to the complicated Phanerozoic geologic activities in South China, and the easily-altered nature of carbonates. The Late Mesozoic remagnetization, not only has been recognized in Doushantuo carbonates (e.g., Gong et al., 2017; Jing et al., 2018), but has been widely observed in many other studies in South China carbonates of different ages (e.g., Kent et al., 1987; Dobson and Heller, 1992; Wang et al., 1993; Huang and Opdyke, 1996; Gong et al., 2017), and is considered to be associated with the Late Mesozoic Yanshanian orogeny. The Silurian remagnetization of Doushantuo carbonates, which has also been reported in several studies (e.g., Macouin et al., 2004; Jing et al., 2015; Zhang et al., 2015), is less well-understood regarding its mechanism. For instance, Zhang et al. (2015) argue that the paleomagnetic results of Macouin et al. (2004) from the Shimen section in Hunan Province are suspicious and might indicate a Silurian remagnetization based on the similarity between the paleomagnetic pole of Macouin et al. (2004) and the Silurian pole of South China. Evan though Macouin et al. (2004) provided a positive fold test to support that their results are primary, the fold was pre-Jurassic, too young to put a strong constraint on the age of magnetization. Therefore, a more rigorous field test is required. Jing et al. (2018) observed a Silurian remagnetization of Doushantuo carbonates from the Qinglinkou and Jiulongwan sections in Hubei Province, and attributed the remagnetization to episodes of hydrocarbon generation, during which time new magnetic minerals precipitated and acquired a secondary magnetization. So far, only results from the Doushantuo Formation in the Jiulongwan section in Hubei Province indicate a primary magnetostratigraphy that has been supported by positive reversal and fold tests (Zhang et al., 2015; Jing et al., 2018). But it is still debatable whether the remanent magnetization in Zhang et al. (2015) has been partially contaminated by the incomplete removal of secondary overprints (Jing et al., 2015). Different from other paleomagnetic studies of Doushantuo carbonates, Zhang et al. (2015) performed thermal demagnetization in a nitrogen atmosphere, which would effectively suppress chemical alteration of magnetic minerals during heating. Also, Valet et al. (1998) show that results of paleointensity studies could be significantly improved by heating in an argon atmosphere instead of air. Therefore, noble gas might be very helpful during thermal demagnetization in order to resolve the magnetization carried by rocks bearing various types of magnetic minerals, and should be considered in future paleomagnetic studies. Besides, early-diagenetic greigite has been observed in the carbonate concretions of Doushantuo Member IV (Dong et al., 2013). Dong et al. (2013) suggest that carbonate concretions could protect the greigite from late diagenesis, which could provide potential opportunities for yielding good paleomagnetic results.

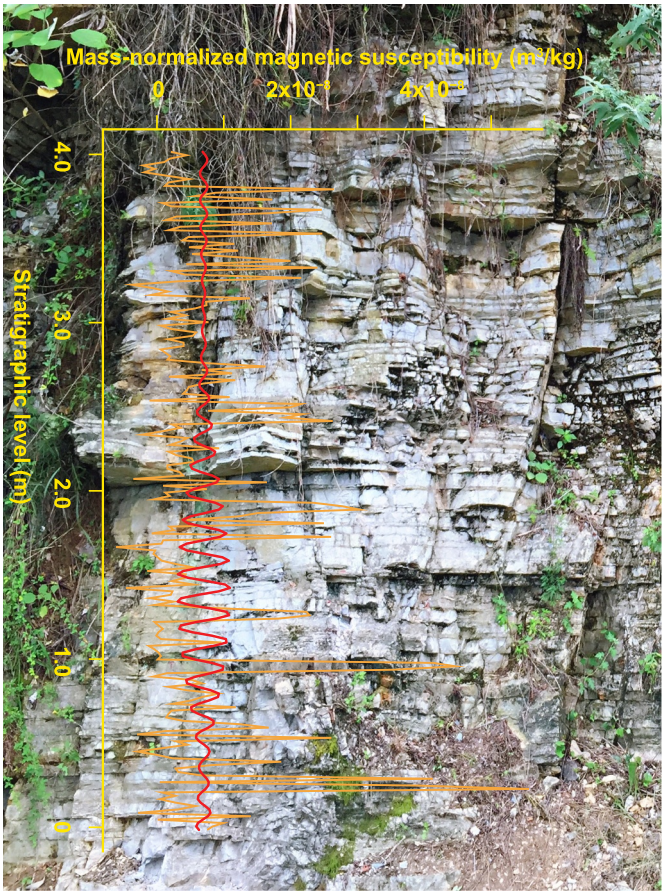

Fig. 11. Comparison between the cyclic color variation of Doushantuo carbonates and MS series. The orange curve is the raw MS series, and the red curve is the filtered MS series at precessional frequencies. (For interpretation of the references to color in this figure legend, the reader is referred to the web version of this article.)

5.2. Encoding mechanism of Milankovitch cycles in Doushantuo carbonates and its implications

MTM spectral analysis of MS series reveals a suite of peaks above the 90% confidence level (Fig. 8). Because MS is dominated by paramagnetic minerals, secondary ferromagnetic minerals (pyrrhotite) only contribute background noise to MS series. That also explains why some spectral peaks only reach 90% significance level. We notice that the ratios of the wavelengths of these significant spectral peaks are similar to the ratios of Milankovitch cycles estimated for the Ediacaran Period (Laskar et al., 2004; Waltham, 2015; Table 2), and argue that the significant spectral peaks are astronomical in origin. ASM analysis yields a SAR of 0.86 cm/kyr for the upper section of the Doushantuo Formation in the Huanglianba section. This SAR is reasonable for a carbonate platform depositional environment (Bosscher and Schlager, 1993), and agrees reasonably with the SAR estimate obtained from the time-equivalent Dongdahe section in Yunnan Province, which is 1.0 cm/kyr (Gong et al., 2017). Given this SAR, we can tentatively estimate the duration of the Shuram CIE. Although the Shuram CIE is not completely recorded in the Huanglianba section, based on the $\delta^{13}C_{VPDB}$ profile, the CIE persists for at least 52 m of stratigraphic thickness, which yields a minimum estimate for its duration of > 6 Myr using 0.82 cm/kyr as the steady SAR. This estimate is consistent with the 8–9 Myr duration estimates from cyclostratigraphic studies (Minguez et al., 2015; Minguez and Kodama, 2017; Gong et al., 2017), and also agrees with independent constraints from the stratigraphic and geochronological interpolation (Zhu et al., 2007), the subsidence analysis (Witkosky and Wernicke, 2018), and the geochemical model (Miyazaki et al., 2018). The consistent duration of the Shuram CIE can also justify the astronomical origin of the peaks revealed by MTM spectral analysis of MS series.

How could Milankovitch cycles be preserved in chemically remagnetized carbonates, with the existence of authigenic magnetic minerals? Since the paramagnetic minerals contribute ~70–95% of the susceptibility (Fig. 7), we argue that it is the concentration variation of paramagnetic minerals that carries the cycles in MS series. Therefore, we propose that during the deposition of Doushantuo carbonates in the Yangtze Platform, Milankovitch cycles controlled and regulated monsoon intensity, which largely influenced the erosion and weathering regimes in South China. As a result, the varying amount of paramagnetic detritus (e.g., clays) transported from the continent to the carbonate platform faithfully recorded the Milankovitch cycles.

To further test the origin of the spectral peaks and their relationship with the depositional process and cyclic color variation of Doushantuo carbonates, we filtered MS series using a Gaussian window centered at the average precessional frequency (6.3 m^{-1}). Compared filtered MS series with the field observation of Doushantuo carbonates, we observed that they generally agree with each other, with high and low MS values corresponding to dark and light carbonate layers, respectively (Fig. 11). Therefore, precessional cycles likely regulated the amount of terrestrial clay minerals transported from the continent and deposited at a background of stable rate of carbonate precipitation, which resulted in the cyclic color variation of Doushantuo carbonates.

In the power spectrum, we also observed two high-frequency peaks, 19.03 m^{-1} and 20.03 m^{-1} (Fig. 8; Table 2). Using a SAR of 0.86 cm/kyr, these two peaks yield a periodicity of ~6 kyr (Table 2). These two peaks are interpreted to be sub-Milankovitch cycles, which are commonly reported in Phanerozoic studies (e.g., Reuning et al., 2006; Wu et al., 2012; Spahn et al., 2013) and have been found in Mesoproterozoic sequence in China as well (Zhang et al., 2015). The origin of sub-Milankovitch cycles is still debated, but it has been suggested to result from: half-precessional cycles because the Sun sweeps across the intertropical zone twice a year (Berger and Loutre, 1997), non-linear feedback to astronomical forcing (Yiou et al., 1991; Willis et al., 1999), and the millennial-scale variations in solar insolation (Wu et al., 2012). Since the periodicity of the sub-Milankovitch cycles observed from the Huanglianba section is ~5–6 kyr, less than the half-precessional periodicity estimated for the Ediacaran Period (Table 2), we suspect that the origin of the sub-Milankovitch cycles could likely be the millennial-scale solar fluctuations, which affected the deposition of Doushantuo carbonates. However, it is also possible that the sub-Milankovitch cycles are half-precessional cycles, but our sampling resolution is not high enough to precisely resolve their periodicities.

A summary of available geochronological constraints from the Doushantuo Formation shows that the lowermost and uppermost parts of the formation have been precisely dated by U–Pb method using zircons in volcanic ash beds (Condon et al., 2005; Zhang et al., 2005; Liu et al., 2009), which yield a ~84 Myr duration for the Doushantuo Formation, ranging from ~635 Ma to ~551 Ma. Published cyclostratigraphic results also focus on the lowermost and uppermost parts of the formation (Fig. 12). For instance, Sui et al. (2018) reported an astronomical time scale for the lowermost Doushantuo Formation by studying the variations of Ca concentration and Fe/Ti ratio of the carbonates. Sui et al. (2018) recognized 27 long-eccentricity (405 kyr) cycles from a 22.3 m section, and obtained the averaged SARs of 0.23 cm/kyr and 0.195 cm/kyr for Doushantuo Members I and II, respectively. Combining U–Pb zircon ages and a SAR of 0.23 cm/kyr, Sui et al. (2018) provided an estimated duration of ~1.6 Myr for the 3.7 m cap carbonates above the Nantuo diamictites, which is consistent with several geomagnetic polarity reversals recognized in Marinoan cap carbonates globally (e.g., Trindade et al., 2003). Using a SAR of 0.195 cm/kyr, Sui et al. (2018) estimated that the negative CIE at the boundary of Doushantuo Members II and III occurred ~20 Myr before

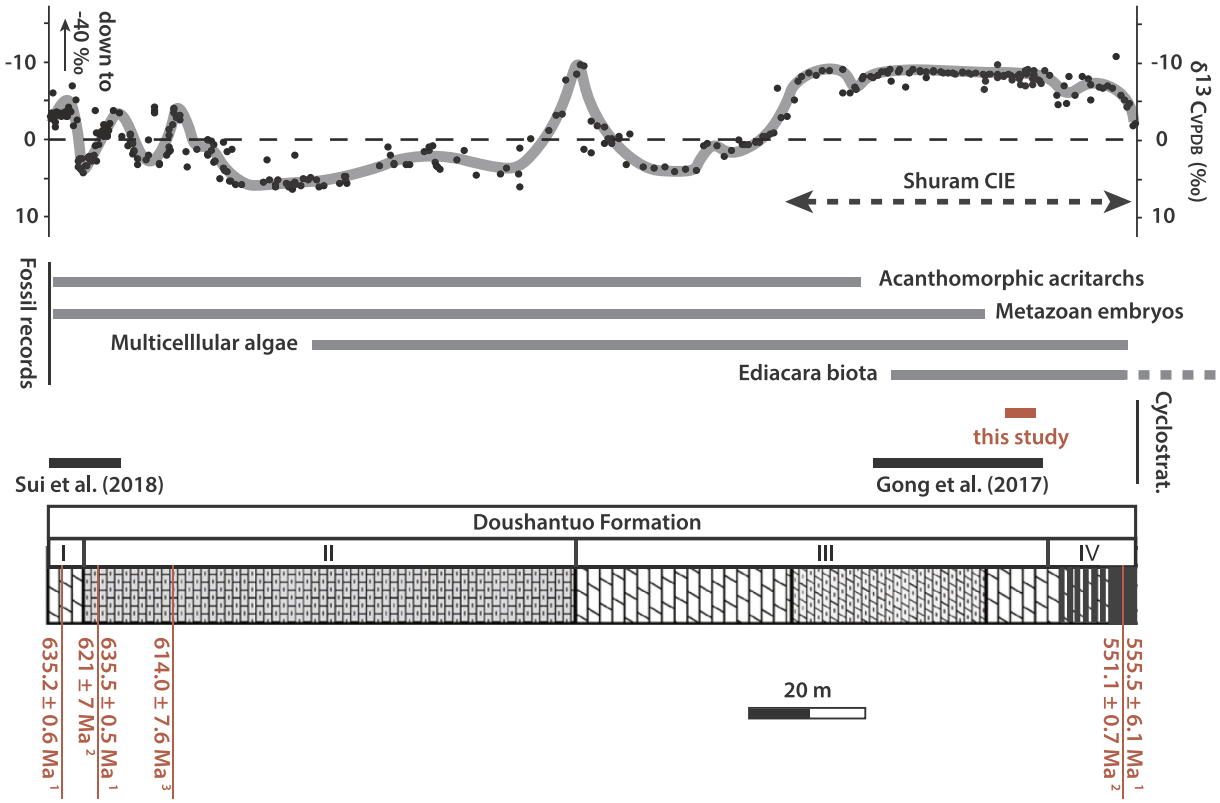

Fig. 12. Summary of geochronological constraints from the Doushantuo Formation. Carbon isotope data and fossil records are from McFadden et al. (2008). The dashed line means that the record of Ediacara biota extends to younger strata, i.e. Dengying Formation. Stratigraphic column is modified from Zhu et al. (2007), using the Jiulongwan section in Hubei Province as a type section. Lithologic legends see Fig. 1C. Stratigraphic positions of cyclostratigraphic samples from Gong et al. (2017) and this study are determined by stratigraphic correlation and by comparing carbon isotope profiles of each study. References for U–Pb zircon ages: 1. Condon et al. (2005); 2. Zhang et al. (2005); 3. Liu et al. (2009). Zircons are from volcanic ash beds in Doushantuo Formation.

the Gaskiers glaciation (~580 Ma; Halverson et al., 2005). On the other hand, Gong et al. (2017) conducted rock magnetic cyclostratigraphy on the uppermost of the formation, and obtained an averaged SAR of 1.0 cm/kyr for Doushantuo Member III. Gong et al. (2017) suggested that the onset age of the Shuram CIE is ~560 Ma based on the SAR of 1.0 cm/kyr, in combination with the U–Pb zircon ages of ~551 Ma at the termination of the Shuram CIE. The result of this study is in an agreement with that of Gong et al. (2017). Hence, Shuram CIE is likely ~20 Myr younger than the Gaskiers glaciation.

Compared to the well-constrained lowermost and uppermost parts of the Doushantuo Formation, the middle part of the formation which archives large fluctuations of carbon isotope values and key fossil records, yet has no age constraint (Fig. 12). Considering the temporal and spatial changes in the depositional environments and lithologies across the Yangtze carbonate platform (Jiang et al., 2011), it is unrealistic and will create large uncertainties to assume a steady SAR for a prolonged duration. In fact, the SARs retrieved from the three cyclostratigraphic studies from the Doushantuo Formation are quite different due to their differences in age, lithology and depositional environment. Therefore, SAR needs to be estimated on a case-by-case basis. Future cyclostratigraphic studies should cover the entire formation, and could provide opportunities to establish a high-resolution depositional history for the Doushantuo Formation.

The success of using rock magnetic cyclostratigraphy on the remagnetized sedimentary sequence of this study sheds light on its chronostratigraphic application to ancient rocks, which to a certain degree, overprinted by later geological processes. Especially for carbonate rocks, which are one of the most significant components of sedimentary rocks and are considered as important archives of seawater chemistry. Many perturbations of seawater chemistry such as the Neoproterozoic Shuram, Bitter Spring and Trezona CIEs (Swanson-Hysell et al., 2010), and the Paleoproterozoic Lomagundi-Jatuli CIE (Melezhik et al., 2007), are considered to have potentially influenced Earth's biotic evolution. High-resolution chronostratigraphy is crucial for understanding the duration and tempo of these perturbations. Even though carbonate rocks are vulnerable to alteration and robust paleomagnetic signals might not be easily resolved, it is still possible to retrieve Milankovitch cycles encoded in rock magnetics of remagnetized carbonates, as long as the remagnetization mechanism and encoding process of Milankovitch cycles are independent. Rock magnetic cyclostratigraphy allows the establishment of a floating astronomical timescale that can be used to estimate the sediment accumulation rates and the duration of geological events, and to construct high-resolution chronostratigraphies, which has wide applications in Precambrian strata.

6. Conclusions

The Ediacaran Doushantuo Formation in the Huanglianba section, Guizhou Province, South China has experienced a Late Triassic remagnetization, which is suggested to be related to the Indosinian orogeny. A detailed characterization of magnetic mineralogy by various rock magnetic experiments and scanning electron microscopic analyses demonstrates that the remagnetization is chemical in origin. Unfortunately, paleomagnetic results of the Ediacaran strata in South China are not robust enough to provide a detailed and reliable magnetostratigraphy for regional and global stratigraphic correlations and comparisons. Future paleomagnetic work is still needed, and should make good use of the ongoing Chinese drilling programs, in order to yield additional sequences of Ediacaran strata and perhaps more

records of ash layers for high-precision U–Pb geochronology. In this study, we also report a successful study of rock magnetic cyclostratigraphy of Doushantuo carbonates, which, even though, were chemically remagnetized. We find that Milankovitch cycles were encoded in the variation of magnetic susceptibility, which is dominated by paramagnetic minerals, such as clays. Our results point out the potential use of rock magnetic cyclostratigraphy for constraining sediment accumulation rates, estimating the duration of geological events and refining chronostratigraphies. Different paleoclimate proxies (e.g. gamma ray, color, grain size, mineralogy, isotopes, geochemical ratios), which could carry astronomically forced climate cycles, should also be considered in addition to magnetic susceptibility in future studies.

Acknowledgements

The authors would like to thank Wenjun Jiao and Boxing Zhang for assistance in field work, Bruce Idleman for carbon isotope measurements and SEM analyses, Junfeng Zhang, Aihua Yang and Xianqing Jing for helpful discussions. We are grateful to Mingsong Li, an anonymous reviewer, and editors Thomas Algeo, David Kemp and Chunju Huang for constructive comments and suggestions that helped improve the manuscript. Support from the National Science Foundation (EAR-1322002) and National Natural Science Foundation of China (No. 41230208) is acknowledged.

Appendix A. Supplementary data

Supplementary data to this article can be found online at https://doi.org/10.1016/j.palaeo.2019.05.002.

References

Abrajevitch, A., Van der Voo, R., 2010. Incompatible Ediacaran paleomagnetic directions suggest an equatorial geomagnetic dipole hypothesis. Earth Planet. Sci. Lett. 293 (1), 164–170.
Bao, X., Zhang, S., Jiang, G., Wu, H., Li, H., Wang, X., ... Yang, T., 2018. Cyclostratigraphic constraints on the duration of the Datangpo Formation and the onset age of the Nantuo (Marinoan) glaciation in South China. Earth Planet. Sci. Lett. 483, 52–63.
Berger, A., Loutre, M.F., 1997. Intertropical latitudes and precessional and half-precessional cycles. Science 278 (5342), 1476–1478.
BGMRGP (Bureau of Geology and Mineral Resources of Guizhou Province), 1987. Regional Geology of Guizhou Province. vol. 698 Geol. Publ. House, Beijing (in Chinese).
Bosscher, H., Schlager, W., 1993. Accumulation rates of carbonate platforms. The Journal of Geology 101 (3), 345–355.
Butler, R.F., 1992. Paleomagnetism: magnetic domains to geologic terranes. vol. 319 Blackwell Scientific Publications, Boston.
Condon, D., Zhu, M., Bowring, S., Wang, W., Yang, A., Jin, Y., 2005. U-Pb ages from the Neoproterozoic Doushantuo Formation. China. Science 308 (5718), 95–98.
Dekkers, M.J., 1989. Magnetic properties of natural pyrrhotite. II. High-and low-temperature behaviour of J_{rs} and TRM as function of grain size. Phys. Earth Planet. Inter. 57 (3–4), 266–283.
Dobson, J.P., Heller, F., 1992. Remagnetization in southeast China and the collision and suturing of the Huanan and Yangtze Blocks. Earth Planet. Sci. Lett. 111 (1), 11–21.
Dong, J., Zhang, S., Jiang, G., Li, H., Gao, R., 2013. Greigite from carbonate concretions of the Ediacaran Doushantuo Formation in South China and its environmental implications. Precambrian Res. 225, 77–85.
Dunlop, D.J., Özdemir, Ö., 2001. Rock Magnetism: Fundamentals and Frontiers. vol. 3 Cambridge University Press.
Fisher, R.A., 1953. Dispersion on a sphere. Proc. R. Soc. Lond. A 217 (1130), 295–305.
Gong, Z., Kodama, K.P., Li, Y.X., 2017. Rock magnetic cyclostratigraphy of the Doushantuo Formation, South China and its implications for the duration of the Shuram carbon isotope excursion. Precambrian Res. 289, 62–74.
Grotzinger, J.P., Fike, D.A., Fischer, W.W., 2011. Enigmatic origin of the largest-known carbon isotope excursion in Earth's history. Nat. Geosci. 4 (5), 285–292.
Gunderson, K.L., Kodama, K.P., Anastasio, D.J., Pazzaglia, F.J., 2013. Rock-magnetic cyclostratigraphy for the Late Pliocene-Early Pleistocene Stirone section, Northern Apennine mountain front, Italy. Geol. Soc. Lond., Spec. Publ. 373 (1), 309–323.
Halverson, G.P., Hoffman, P.F., Schrag, D.P., Maloof, A.C., Rice, A.H.N., 2005. Toward a Neoproterozoic composite carbon-isotope record. GSA Bull. 117 (9–10), 1181–1207.
Han, S., Zhang, J., Li, Y., Horsfield, B., Tang, X., Jiang, W., Chen, Q., 2013. Evaluation of lower Cambrian shale in northern Guizhou province, South China: Implications for shale gas potential. Energy Fuel 27 (6), 2933–2941.
Hrouda, F., Jelínek, V., Zapletal, K., 1997. Refined technique for susceptibility resolution into ferromagnetic and paramagnetic components based on susceptibility temperature-variation measurement. Geophys. J. Int. 129 (3), 715–719.
Huang, K., Opdyke, N.D., 1996. Severe remagnetization revealed from Triassic platform carbonates near Guiyang, Southwest China. Earth Planet. Sci. Lett. 143 (1–4), 49–61.
Jiang, G., Shi, X., Zhang, S., Wang, Y., Xiao, S., 2011. Stratigraphy and paleogeography of the Ediacaran Doushantuo Formation (ca. 635-551 Ma) in south China. Gondwana Res. 19 (4), 831–849.
Jiao, W.J., Li, Y.X., Yang, Z.Y., 2018. Paleomagnetism of a well-dated marine succession in South China: a possible Late Cambrian true polar wander (TPW). Phys. Earth Planet. Inter. 277, 38–54.
Jiao, W., Li, Y.X., Yang, Z., Liu, J., 2019. A widespread Early Mesozoic remagnetization in South China. Journal of Geophysical Research: Solid Earth 124, 88–103.
Jing, X., Yang, Z., Tong, Y., Han, Z., 2015. A revised paleomagnetic pole from the mid-Neoproterozoic Liantuo Formation in the Yangtze block and its paleogeographic implications. Precambrian Res. 268, 194–211.
Jing, X., Yang, Z., Tong, Y., Wang, H., Xu, Y., 2018. Identification of multiple magnetizations of the Ediacaran strata in South China. Geophys. J. Int. 212 (1), 54–75.
Kendall, B., Komiya, T., Lyons, T.W., Bates, S.M., Gordon, G.W., Romaniello, S.J., ... Sawaki, Y., 2015. Uranium and molybdenum isotope evidence for an episode of widespread ocean oxygenation during the late Ediacaran Period. Geochim. Cosmochim. Acta 156, 173–193.
Kent, D.V., Zeng, X., Wen, Y.Z., Opdyke, N.D., 1987. Widespread late Mesozoic to Recent remagnetization of Paleozoic and lower Triassic sedimentary rocks from South China. Tectonophysics 139 (1–2), 133–143.
Kirschvink, J.L., 1980. The least-squares line and plane and the analysis of paleomagnetic data. Geophys. J. Int. 62 (3), 699–718.
Knoll, A., Walter, M., Narbonne, G., Christie-Blick, N., 2006. The Ediacaran Period: a new addition to the geologic time scale. Lethaia 39 (1), 13–30.
Kodama, K.P., Hinnov, L.A., 2014. Rock Magnetic Cyclostratigraphy. John Wiley & Sons.
Kodama, K.P., Anastasio, D.J., Newton, M.L., Pares, J.M., Hinnov, L.A., 2010. High-resolution rock magnetic cyclostratigraphy in an Eocene flysch, Spanish Pyrenees. Geochem. Geophys. Geosyst. 11 (6).
Kruiver, P.P., Dekkers, M.J., Heslop, D., 2001. Quantification of magnetic coercivity components by the analysis of acquisition curves of isothermal remanent magnetisation. Earth Planet. Sci. Lett. 189 (3–4), 269–276.
Laskar, J., Robutel, P., Joutel, F., Gastineau, M., Correia, A.C.M., Levrard, B., 2004. A long-term numerical solution for the insolation quantities of the Earth. Astronomy & Astrophysics 428 (1), 261–285.
Li, Z.X., Wartho, J.A., Occhipinti, S., Zhang, C.L., Li, X.H., Wang, J., Bao, C., 2007. Early history of the eastern Sibao Orogen (South China) during the assembly of Rodinia: New mica $^{40}Ar/^{39}Ar$ dating and SHRIMP U-Pb detrital zircon provenance constraints. Precambrian Res. 159 (1–2), 79–94.
Li, C., Love, G.D., Lyons, T.W., Fike, D.A., Sessions, A.L., Chu, X., 2010. A stratified redox model for the Ediacaran ocean. Science 328 (5974), 80–83.
Liu, P., Yin, C., Gao, L., Tang, F., Chen, S., 2009. New material of microfossils from the Ediacaran Doushantuo Formation in the Zhangcunping area, Yichang, Hubei Province and its zircon SHRIMP U-Pb age. Chin. Sci. Bull. 54 (6), 1058–1064.
Lowrie, W., 1990. Identification of ferromagnetic minerals in a rock by coercivity and unblocking temperature properties. Geophys. Res. Lett. 17 (2), 159–162.
Lu, M., Zhu, M., Zhang, J., Shields-Zhou, G., Li, G., Zhao, F., ... Zhao, M., 2013. The DOUNCE event at the top of the Ediacaran Doushantuo Formation, South China: Broad stratigraphic occurrence and non-diagenetic origin. Precambrian Res. 225, 86–109.
Lurcock, P.C., Wilson, G.S., 2012. PuffinPlot: a versatile, user-friendly program for paleomagnetic analysis. Geochem. Geophys. Geosyst. 13 (6).
Macouin, M., Besse, J., Ader, M., Gilder, S., Yang, Z., Sun, Z., Agrinier, P., 2004. Combined paleomagnetic and isotopic data from the Doushantuo carbonates, South China: implications for the “snowball Earth” hypothesis. Earth Planet. Sci. Lett. 224 (3), 387–398.
Mann, M.E., Lees, J.M., 1996. Robust estimation of background noise and signal detection in climatic time series. Clim. Chang. 33 (3), 409–445.
McCabe, C., Elmore, R.D., 1989. The occurrence and origin of late Paleozoic remagnetization in the sedimentary rocks of North America. Rev. Geophys. 27 (4), 471–494.
McFadden, K.A., Huang, J., Chu, X., Jiang, G., Kaufman, A.J., Zhou, C., ... Xiao, S., 2008. Pulsed oxidation and biological evolution in the Ediacaran Doushantuo Formation. Proc. Natl. Acad. Sci. 105 (9), 3197–3202.
Melezhik, V.A., Huhma, H., Condon, D.J., Fallick, A.E., Whitehouse, M.J., 2007. Temporal constraints on the Paleoproterozoic Lomagundi-Jatuli carbon isotopic event. Geology 35 (7), 655–658.
Meyers, S.R., 2014. Astrochron: An R Package for Astrochronology. https://cran.r-project.org/web/packages/astrochron/index.html.
Meyers, S.R., Sageman, B.B., 2007. Quantification of deep-time orbital forcing by average spectral misfit. Am. J. Sci. 307 (5), 773–792.
Minguez, D., Kodama, K.P., 2017. Rock magnetic chronostratigraphy of the Shuram carbon isotope excursion: Wonoka Formation, Australia. Geology 45 (6), 567–570.
Minguez, D., Kodama, K.P., Hillhouse, J.W., 2015. Paleomagnetic and cyclostratigraphic constraints on the synchroneity and duration of the Shuram carbon isotope excursion, Johnnie Formation, Death Valley Region, CA. Precambrian Res. 266, 395–408.
Miyazaki, Y., Planavsky, N., Bolton, E.W., Reinhard, C.T., 2018. Making sense of massive carbon isotope excursions with an inverse carbon cycle model. Journal of Geophysical Research: Biogeosciences 123 (8), 2485–2496.
Peters, C., Dekkers, M.J., 2003. Selected room temperature magnetic parameters as a function of mineralogy, concentration and grain size. Physics and Chemistry of the Earth, Parts A/B/C 28 (16–19), 659–667.
Pullaiah, G., Irving, E., Buchan, K.L., Dunlop, D.J., 1975. Magnetization changes caused by burial and uplift. Earth Planet. Sci. Lett. 28 (2), 133–143.

Reuning, L., Reijmer, J.J., Betzler, C., Timmermann, A., Steph, S., 2006. Sub-Milankovitch cycles in periplatform carbonates from the early Pliocene Great Bahama Bank. Paleoceanography and Paleoclimatology 21 (1).
Shi, W., Li, C., Luo, G., Huang, J., Algeo, T.J., Jin, C., ... Cheng, M., 2018. Sulfur isotope evidence for transient marine-shelf oxidation during the Ediacaran Shuram Excursion. Geology 46 (3), 267–270.
Spahn, Z.P., Kodama, K.P., Preto, N., 2013. High-resolution estimate for the depositional duration of the Triassic Latemar Platform: a new magnetostratigraphy and magnetic susceptibility cyclostratigraphy from basinal sediments at Rio Sacuz, Italy. Geochem. Geophys. Geosyst. 14 (4), 1245–1257.
Sui, Y., Huang, C., Zhang, R., Wang, Z., Ogg, J., Kemp, D.B., 2018. Astronomical time scale for the lower Doushantuo Formation of early Ediacaran, South China. Science Bulletin 63 (22), 1485–1494.
Swanson-Hysell, N.L., Rose, C.V., Calmet, C.C., Halverson, G.P., Hurtgen, M.T., Maloof, A.C., 2010. Cryogenian glaciation and the onset of carbon-isotope decoupling. Science 328 (5978), 608–611.
Thomson, D.J., 1982. Spectrum estimation and harmonic analysis. Proc. IEEE 70 (9), 1055–1096.
Trindade, R.I.F.D., Font, E., D'Agrella-Filho, M.S., Nogueira, A.C.R., Riccomini, C., 2003. Low-latitude and multiple geomagnetic reversals in the Neoproterozoic Puga cap carbonate, Amazon craton. Terra Nova 15 (6), 441–446.
Valet, J.P., Tric, E., Herrero-Bervera, E., Meynadier, L., Lockwood, J.P., 1998. Absolute paleointensity from Hawaiian lavas younger than 35 ka. Earth Planet. Sci. Lett. 161 (1), 19–32.
Waltham, D., 2015. Milankovitch period uncertainties and their impact on cyclostratigraphy. J. Sediment. Res. 85 (8), 990–998.
Wang, Z., Van der Voo, R., Wang, Y., 1993. A new Mesozoic apparent polar wander loop for South China: paleomagnetism of Middle Triassic rocks from Guizhou Province. Earth Planet. Sci. Lett. 115 (1–4), 1–12.
Wang, Y., Fan, W., Zhang, G., Zhang, Y., 2013. Phanerozoic tectonics of the South China Block: key observations and controversies. Gondwana Res. 23 (4), 1273–1305.
Willis, K.J., Kleczkowski, A., Briggs, K.M., Gilligan, C.A., 1999. The role of sub-Milankovitch climatic forcing in the initiation of the Northern Hemisphere glaciation. Science 285 (5427), 568–571.
Witkosky, R., Wernicke, B.P., 2018. Subsidence history of the Ediacaran Johnnie Formation and related strata of southwest Laurentia: Implications for the age and duration of the Shuram isotopic excursion and animal evolution. Geosphere 14 (5), 2245–2276.
Wu, H., Zhang, S., Feng, Q., Jiang, G., Li, H., Yang, T., 2012. Milankovitch and sub-Milankovitch cycles of the early Triassic Daye Formation, South China and their geochronological and paleoclimatic implications. Gondwana Res. 22 (2), 748–759.
Xiao, S., Laflamme, M., 2009. On the eve of animal radiation: phylogeny, ecology and evolution of the Ediacara biota. Trends in Ecology and Evolution 24 (1), 31–40.
Xiao, S., McFadden, K.A., Peek, S., Kaufman, A.J., Zhou, C., Jiang, G., Hu, J., 2012. Integrated chemostratigraphy of the Doushantuo Formation at the northern Xiaofenghe section (Yangtze Gorges, South China) and its implication for Ediacaran stratigraphic correlation and ocean redox models. Precambrian Res. 192, 125–141.
Yiou, P., Genthon, C., Ghil, M., Jouzel, J., Le Treut, H., Barnola, J.M., ... Korotkevitch, Y.N., 1991. High-frequency paleovariability in climate and CO_2 levels from Vostok ice core records. Journal of Geophysical Research: Solid Earth 96 (B12), 20365–20378.
Zhang, S., Jiang, G., Zhang, J., Song, B., Kennedy, M.J., Christie-Blick, N., 2005. U-Pb sensitive high-resolution ion microprobe ages from the Doushantuo Formation in south China: Constraints on late Neoproterozoic glaciations. Geology 33 (6), 473–476.
Zhang, S., Li, H., Jiang, G., Evans, D.A., Dong, J., Wu, H., ... Xiao, Q., 2015. New paleomagnetic results from the Ediacaran Doushantuo Formation in South China and their paleogeographic implications. Precambrian Res. 259, 130–142.
Zhang, Y., Jia, D., Yin, H., Liu, M., Xie, W., Wei, G., Li, Y., 2016. Remagnetization of lower Silurian black shale and insights into shale gas in the Sichuan Basin, south China. J. Geophys. Res. Solid Earth 121 (2), 491–505.
Zhao, X., Coe, R.S., 1987. Palaeomagnetic constraints on the collision and rotation of North and South China. Nature 327 (6118), 141–144.
Zhu, M., Zhang, J., Yang, A., 2007. Integrated Ediacaran (Sinian) chronostratigraphy of South China. Paleogeography, Paleoclimatology, Paleoecology 254 (1–2), 7–61.
Zijderveld, J.D.A., 1967. AC demagnetization of rocks: analysis of results. Methods in Paleomagnetism 3, 254.